# Ultrafast dynamics and phase changes in crystalline and amorphous GaAs

A. M.-T. Kim, J. P. Callan, C. A. D. Roeser, and E. Mazur
*Harvard University, Division of Engineering & Applied Sciences and Department of Physics, 9 Oxford St, Cambridge, Massachusetts 02138*
(Received 3 April 2002; revised manuscript received 19 September 2002; published 13 December 2002)

The femtosecond-time-resolved response of the spectral dielectric function provides a great wealth of information on carrier and lattice dynamics in highly photoexcited semiconductors. We present measurements of the dielectric function of crystalline and amorphous GaAs over a broad spectral energy range (1.7–3.4 eV), with sub-100-fs time resolution. A detailed analysis of the data reveals many insights into the dynamics and phase changes in semiconductors at high excitation fluences up to and beyond the damage threshold.

DOI: 10.1103/PhysRevB.66.245203 PACS number(s): 78.47.+p

## I. INTRODUCTION

Ultrafast electron and lattice dynamics in semiconductors have been studied extensively since the availability of femtosecond laser pulses.[1,2] Many experiments and theories have increased our knowledge of semiconductors ranging from estimates of fundamental quantities such as electron-phonon scattering times to the generation and detection of Bloch oscillations in superlattices.[3] Not only has this research led to a deeper understanding of fundamental semiconductor physics, but it has also enabled widespread applications such as high-speed optical modulators.[4,5]

Most experiments to date have concentrated on a specific process such as the scattering time of an excited electron with a LO phonon in gallium arsenide (GaAs).[6] In order to observe such specific processes it is necessary to choose an appropriate optical signature. A variety of detection geometries ranging from differential transmission setups to four-wave mixing experiments have been used to measure specific ultrafast processes in semiconductors.[3] In order to minimize the noise due to other competing processes these experiments are usually carried out at relatively low carrier densities ($10^{16}$–$10^{18}$ cm$^{-3}$).

Only a limited amount of work has been done in the regime of highly excited carrier densities ($10^{19}$–$10^{22}$ cm$^{-3}$). This regime is an interesting one for the study of ultrafast processes in semiconductors because many different scattering phenomena occur, challenging researchers to identify the dominant processes that drive the electron and lattice dynamics. It is also increasingly important in modern applications. For example, injection currents in high-power laser diodes create high carrier densities on the order of $10^{18}$ cm$^{-3}$.[7] Also, micromachining using femtosecond lasers, which involves creating extremely high carrier densities (greater than $10^{22}$ cm$^{-3}$), is rapidly moving into commercial applications.[8] To optimize such applications it is necessary to understand the carrier and lattice dynamics at excitation densities close to and beyond the damage threshold (around $10^{22}$ cm$^{-3}$ in GaAs).

In this paper we present femtosecond-time-resolved measurements of the dielectric function of crystalline GaAs ($c$-GaAs) and amorphous GaAs ($a$-GaAs) at carrier densities below and above the threshold for permanent damage. The spectral dielectric function $\epsilon(\omega)$ of a material is an excellent quantity to measure because it contains information on the electronic configuration as well as on the structure of the material. A direct comparison of the crystalline and amorphous phases leads to insights into the nonthermal phase transition each of the materials undergoes upon laser irradiation.

## II. TECHNIQUE

All the dielectric function data presented in this paper were obtained using femtosecond-time-resolved ellipsometry.[9,10] This technique allows direct measurement of the real and imaginary parts of the dielectric function of a material with fs time resolution over a broad energy range (from 1.7 eV to 3.4 eV). We combine multiangle ellipsometry[11] with a white-light pump-probe measurement.[3] By performing broadband time-resolved reflectivity experiments at two different angles under the same excitation conditions, we obtain two reflectivity values for each wavelength and time delay. We account for the chirp of the white light by measuring the chirp in an independent measurement and time shifting the reflectivity data accordingly. If the two angles are chosen appropriately, one can uniquely invert the Fresnel reflectivity formulas to obtain the real and imaginary parts of the spectral dielectric function $\epsilon(\omega)$.[9,10]

For the experiments on $c$-GaAs we used an amplified dye-laser system producing 70-fs, 100-$\mu$J pulses at a repetition rate of 10 Hz and a spectral energy of 1.9 eV. The pump beam was $p$ polarized with an angle of incidence on the sample of 43°. For the experiments on $a$-GaAs we used an amplified Ti:sapphire laser system producing 50-fs, 0.5-mJ pulses at a repetition rate of 1 kHz and a spectral energy of 1.5 eV; the pump beam was $s$ polarized with an angle of incidence of 50°. The angles of the probe beams were 58° and 76° for $c$-GaAs and 53° and 78° for $a$-GaAs.

## III. RESULTS

We used a commercially available $c$-GaAs (100) sample (Cr doped, $\rho > 7\times10^5$ Ω m). The $a$-GaAs sample was created by three stages of ion implantation with Kr ions into a crystalline wafer.

The total dose of $7\times10^{15}$ ions per cm$^2$ constitutes less than 1% of the atoms in the amorphized region of the material. After implantation the material is amorphous down to a

 

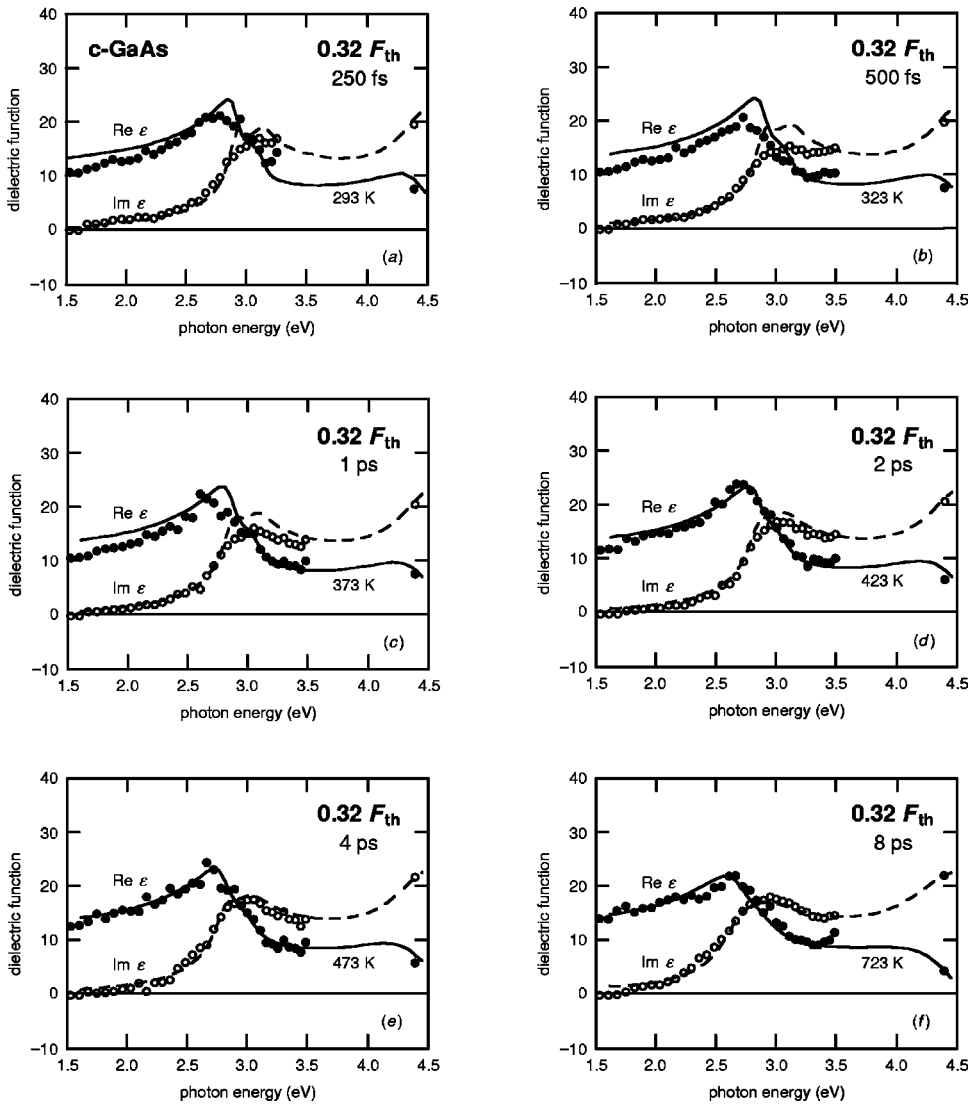


FIG. 1. Evolution of the dielectric function of crystalline GaAs ($\bullet = \mathrm{Re}[\epsilon(\omega)]$, $\circ = \mathrm{Im}[\epsilon(\omega)]$) after excitation at $0.32F_{\mathrm{th}}$. The curves show $\mathrm{Re}[\epsilon(\omega)]$ (solid line) and $\mathrm{Im}[\epsilon(\omega)]$ (dashed line) for *c*-GaAs heated to various temperatures: (a) 293 K, (b) 323 K, (c) 373 K, (d) 423 K, (e) 473 K, and (f) 723 K (Ref. 14). The temperatures are selected by matching curves to the data (for 4 ps and after) or derived from the exponential curves for lattice temperature versus time delay shown in Fig. 2.

depth of 600 nm, which is greater than the optical penetration depth of our probe pulse.

The response of *c*-GaAs and *a*-GaAs to excitation by a femtosecond pulse varies strongly with incident excitation fluence *F*. Above a certain threshold fluence, the samples are permanently damaged, as observed under an optical microscope. Measured in terms of the peak fluence at the center of the Gaussian profile, the threshold for *c*-GaAs is $F_{\text{th-}c} = 1.0$ kJ/m$^2$ and for *a*-GaAs is $F_{\text{th-}a} = 0.1$ kJ/m$^2$.

### A. Low-fluence regime

#### 1. *Crystalline gallium arsenide* ($F < 0.5F_{th\text{-}c}$)

Figure 1 shows the evolution of the dielectric function of *c*-GaAs after excitation by a pulse of peak fluence 0.32 kJ/m$^2$, representative of the low-fluence regime for this material. In addition to the data from the broadband probe, the figure includes data points from a separate measurement of the dielectric function at 4.4 eV.[12] The solid and dashed curves in each of the panels represent the real and imaginary parts of the dielectric function of unexcited *c*-GaAs at various temperatures.[13,14] For clarity we have omitted the error bars for the dielectric function data in this and the following graphs. In most of the graphs, the error bars are on the order of the marker size.[10]

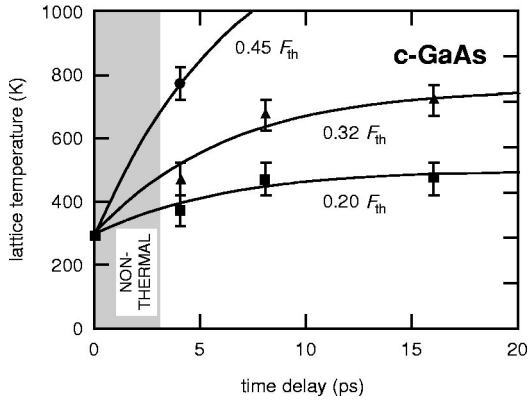


FIG. 2. Laser-induced lattice heating of *c*-GaAs for three different excitations in the low-fluence regime: $0.20F_{\mathrm{th}}$ ($\bullet$), $0.32F_{\mathrm{th}}$ ($\blacktriangle$), and $0.45F_{\mathrm{th}}$ ($\blacksquare$). The fitted exponential curves yield a common rise time of about 7 ps.

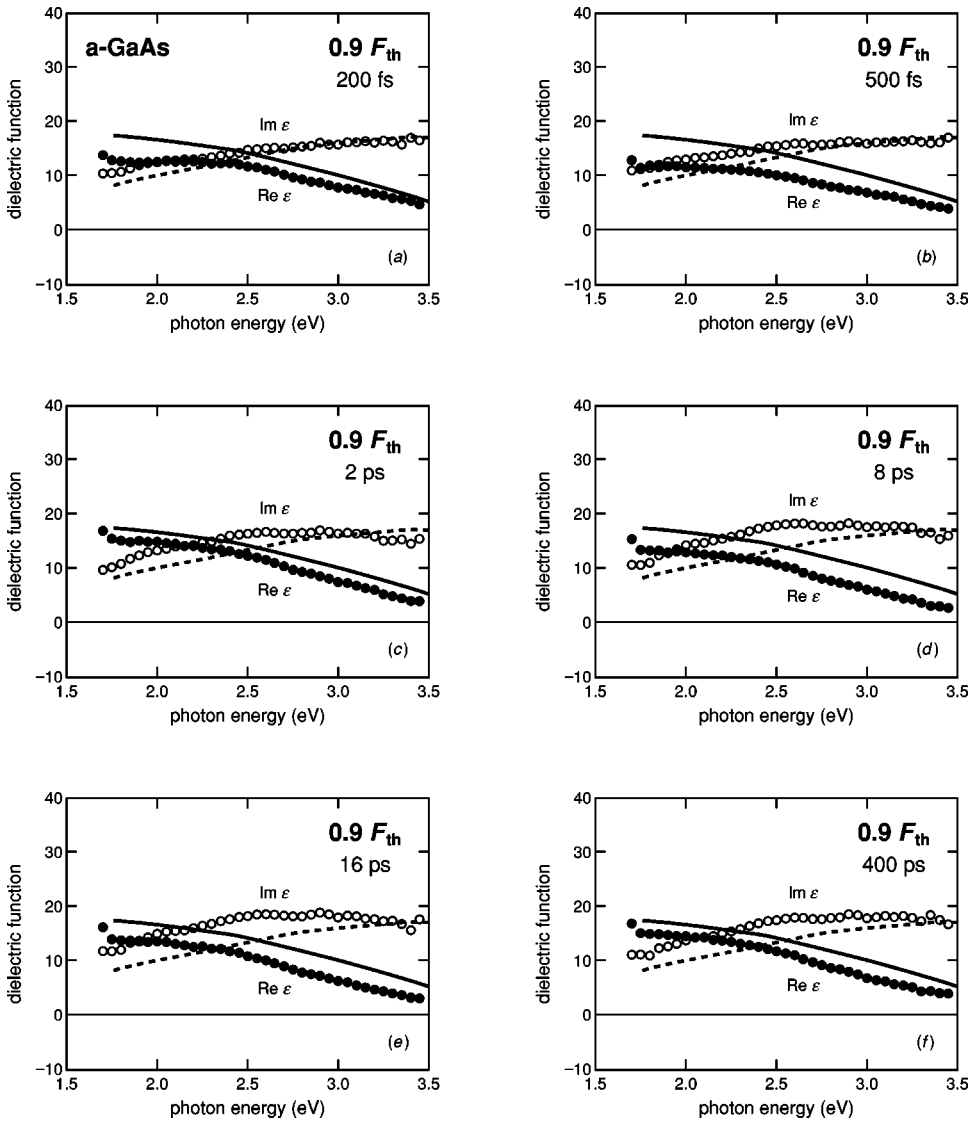


FIG. 3. Evolution of the dielectric function of *a*-GaAs (● $=\mathrm{Re}[\epsilon(\omega)]$, ○ $=\mathrm{Im}[\epsilon(\omega)]$) after excitation by pulses of about $0.9F_{\text{th-}a}$. The dielectric function of *a*-GaAs at room temperature (Ref. 15) is shown for comparison in all panels (solid curves $=\mathrm{Re}[\epsilon(\omega)]$, dashed curves $=\mathrm{Im}[\epsilon(\omega)]$).

For the first 500 fs after excitation, the peak of $\mathrm{Im}[\epsilon(\omega)]$ falls by about 15%–20% in amplitude and broadens slightly. The dispersive ''wiggle'' in $\mathrm{Re}[\epsilon(\omega)]$ flattens out, as expected from the Kramers-Kronig relations. Although the dielectric function partly recovers after about 1 ps, the data do not indicate a return to the original state of the material. The data at 4 and 8 ps agree well with cw-ellipsometric data of the dielectric function of *c*-GaAs at 473 K and 732 K, respectively,[14] as indicated in Figs. 1(e) and 1(f). The lattice heating after 4 ps, indicated by the fits in Fig. 1, is typical of the low-fluence regime.

Figure 2 shows the lattice temperature versus time delay for three different excitation fluences, obtained from matches such as those in Figs. 1(e) and 1(f). As expected, higher excitation fluences lead to higher lattice temperatures. Up to 3 ps, the dielectric function of laser-excited *c*-GaAs still shows contributions due to the excited free carriers and is not solely altered by lattice heating. In addition, we cannot determine the temperature at 8 and 16 ps for $0.45F_{\text{th}}$ because measurements of the dielectric function of *c*-GaAs have only been reported up to 884 K. Exponential fits to the data at $0.20F_{\text{th}}$ and $0.32F_{\text{th}}$ yield a rise time of about 7 ps. These exponential fits can be used to determine the lattice temperatures at times less than 4 ps, when electronic effects also contribute to the dielectric function. In each of the panels (a)–(d) of Fig. 1, the curves represent the published dielectric function[14] for *c*-GaAs at a lattice temperature determined in this fashion. The difference between the data and the curves is due to electronic effects. We shall make use of these difference spectra in Sec. IV A 1 to study the electron dynamics.

### *2. Amorphous gallium arsenide* ($F<1.7F_{th\text{-}a}$)

We confirmed in a separate measurement (not shown here) that the dielectric function of our *a*-GaAs sample agrees with that of an amorphous GaAs sample generated by bombardment with 270-keV $As^+$ ions.[15] Figure 3 shows the evolution of the dielectric function of *a*-GaAs following an excitation of $0.9F_{\text{th}}$. Within the first few hundred femtoseconds, $\mathrm{Im}[\epsilon(\omega)]$ rises and $\mathrm{Re}[\epsilon(\omega)]$ falls for frequencies at the lower end of the spectral range.

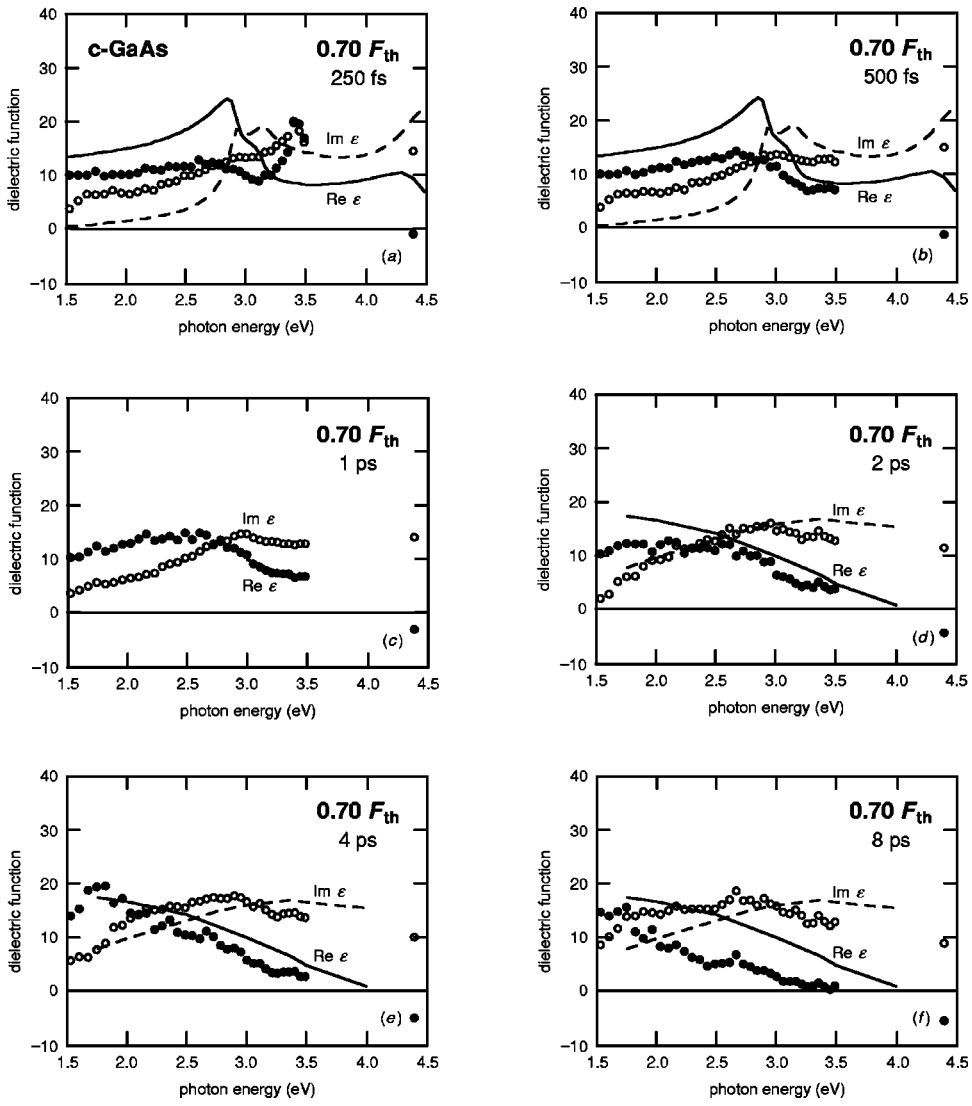


FIG. 4. Evolution of the dielectric function of *c*-GaAs (● = Re[$\epsilon(\omega)$], ○ = Im[$\epsilon(\omega)$]) after excitation at $0.70F_{\text{th-}c}$. The curves in (a) and (b) show Re[$\epsilon(\omega)$] (solid line) and Im[$\epsilon(\omega)$] (dashed line) for *c*-GaAs at room temperature (Ref. 13). The curves in (d), (e), and (f) represent the dielectric function of amorphous GaAs at room temperature (Ref. 15).

The peak in Im[$\epsilon(\omega)$] shifts below its initial position of 3.35 eV, reaching 2.8 eV at 50 ps. Re[$\epsilon(\omega)$] also shifts to lower frequency with time. Such a redshift is expected when a semiconductor heats up.[15–18] We cannot determine the temperature as a function of time delay because the linear optical properties of hot *a*-GaAs have never been measured. However, the evolution of $\epsilon(\omega)$ in Fig. 3 indicates that lattice heats for tens of picoseconds, then starts to cool again on a time scale of several hundred picoseconds, with the dielectric function moving back to higher photon energies. The cooling is due to thermal diffusion, and the time scale of several 100 ps is consistent with theoretical estimates for heat diffusion over tens of nanometers.[19]

### B. Medium-fluence regime

#### 1. Crystalline gallium arsenide ($0.5F_{th\text{-}c} < F < 0.8F_{th\text{-}c}$)

As the data obtained at $0.7F_{\text{th-}c}$ in Fig. 4 show, the changes in $\epsilon(\omega)$ in this fluence regime are more pronounced than in the low-fluence range. The drop in the real part during the first few hundred femtoseconds is larger (cf. Fig. 1), and there is a dramatic increase in the imaginary part for photon energies up to 2.7 eV. Over several picoseconds, we observe the development of a single broad peak in Im[$\epsilon(\omega)$], its center shifting towards lower energy. After 4 ps the peak has moved to about 2.8 eV (from its initial value of 3.1 eV) and its full width at half maximum is greater than 2.8 eV (compared to 0.7 eV initially). Meanwhile, the real part develops a negative slope across most of the frequency range.

The dielectric function at these times is similar to that for amorphous GaAs at room temperature,[15] as demonstrated in Figs. 4(d)–4(f), but the data are shifted towards lower energies, as might be expected because the laser-excited material is heated well above room temperature. Measurements of second-harmonic generation[20] and of the second-order susceptibility[21] indicate that GaAs becomes centrosymmetric (on length scales shorter than or equal to the probe wavelength) a few picoseconds after excitation in this fluence range. Because it is not possible to form a centrosymmetric crystalline phase in GaAs, these data imply a loss of ordering on length scales up to 500–1000 nm. Our experiments on amorphous GaAs provide further evidence that supports amorphization, as we will show in Sec. IV B 2.

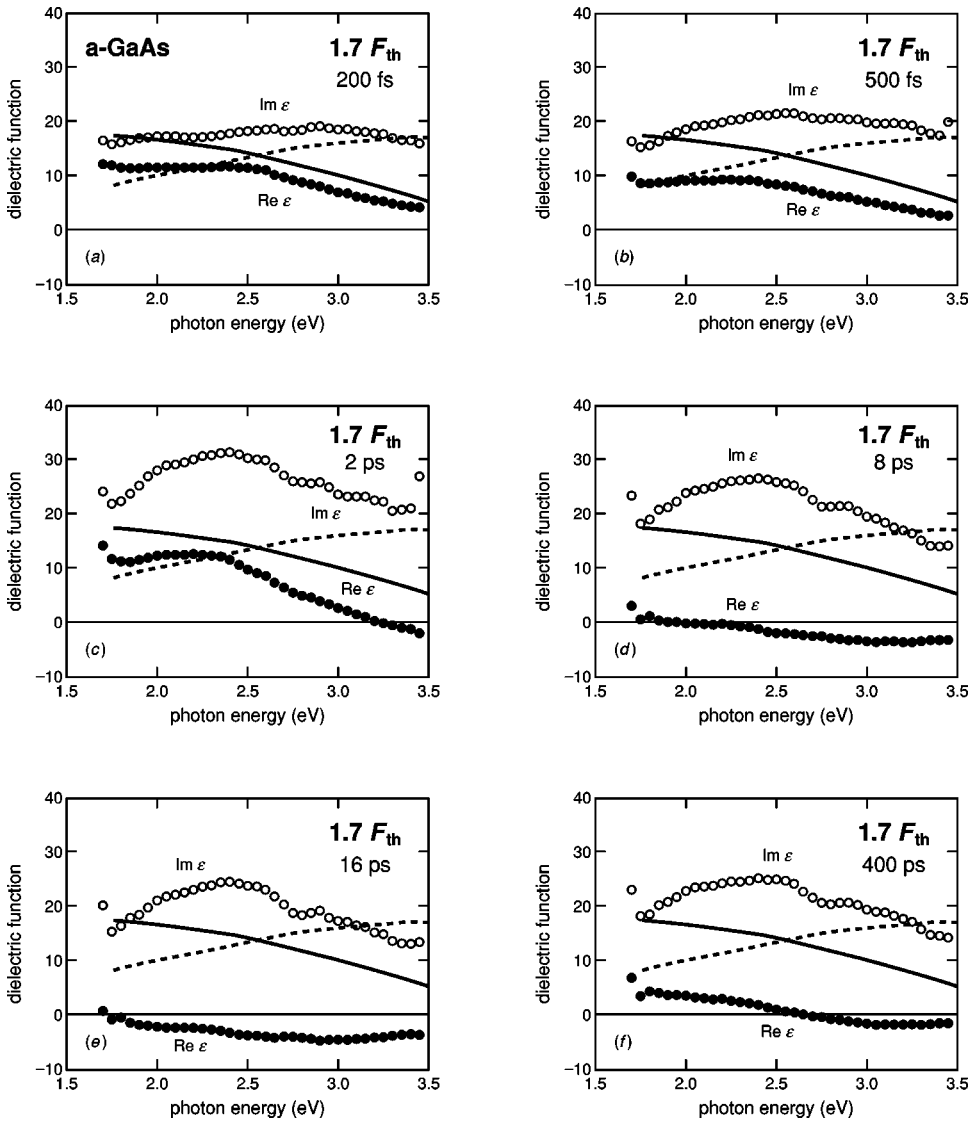


FIG. 5. Evolution of the dielectric function of *a*-GaAs (● = Re[ $\epsilon(\omega)$ ], ○ = Im[ $\epsilon(\omega)$ ]) after excitation at $1.7F_{\text{th-}a}$. The dielectric function of *a*-GaAs at room temperature (Ref. 15) appears for comparison in all panels (solid curves = Re[ $\epsilon(\omega)$ ], dashed curves = Im[ $\epsilon(\omega)$ ]).

#### *2. Amorphous gallium arsenide* ($F \approx 1.7F_{th\text{-}a}$)

For *a*-GaAs we do not observe a clearly distinct intermediate region. Instead we present data obtained at $F = 1.7F_{\text{th-}a}$, on the border between the low- and high-fluence regimes. Figure 5 shows the evolution of $\epsilon(\omega)$ at $F = 1.7F_{\text{th-}a}$. The initial electronic effects are greater than at $0.9F_{\text{th-}a}$. After 2 ps, the peak value of Im[ $\epsilon(\omega)$ ] has increased to a value of 30, and both the peak of Im[ $\epsilon(\omega)$ ] and the zero crossing of Re[ $\epsilon(\omega)$ ] have moved to lower photon energy. The zero crossing of Re[ $\epsilon(\omega)$ ] continues to drop in frequency over the following picoseconds, while Im[ $\epsilon(\omega)$ ] takes on a Drude-like shape.[22] After 16 ps, Re[ $\epsilon(\omega)$ ] is negative across the entire spectral range. Although Im[ $\epsilon(\omega)$ ] still has a peak around 2.4 eV, the dielectric function looks like one produced by the Drude model for a free-electron gas.

### C. High-fluence regime

#### *1. Crystalline gallium arsenide* ($F > 0.8F_{th\text{-}c}$)

Above $0.80F_{\text{th-}c}$, the evolution of $\epsilon(\omega)$ is very different from that in the lower-fluence regimes. The real part of the dielectric function becomes negative over the entire observed spectral range, and the photon energy at which Re[ $\epsilon(\omega)$ ] crosses zero decreases with time delay, as shown in Fig. 6. The zero crossing of the real part of the dielectric function coincides with the main resonance in a material—that is, the transition in the system with the dominant oscillator strength.[23] In *c*-GaAs this transition corresponds to the $E_2$ peak in Im[ $\epsilon(\omega)$ ] which is due to the large joint density of states around the *X* valley in the Brillouin zone.[24] The location of $E_2$ approximately gives the value of the average bonding-antibonding splitting of GaAs.[23] Thus, Fig. 6(a) shows that, at $F = 1.60F_{\text{th-}c}$, most of the oscillator strength moves from an initial value of 4.75 eV (Ref. 13) to below 3.2 eV within 250 fs. By 4 ps, the zero crossing of the real part has shifted to well below 2 eV. The curves in panels (d)–(f) of Fig. 6 show fits to a Drude model. All fits have a relaxation time of 0.18 fs and plasma frequencies of 13.0, 12.0, and 10.5 eV, respectively. A plasma frequency of 10 eV corresponds to a free carrier density of $N = 0.73 \times 10^{23}$ cm$^{-3}$. Given that the total density of all valence electrons in *c*-GaAs is $1.12 \times 10^{23}$ cm$^{-3}$, the value we find for the plasma

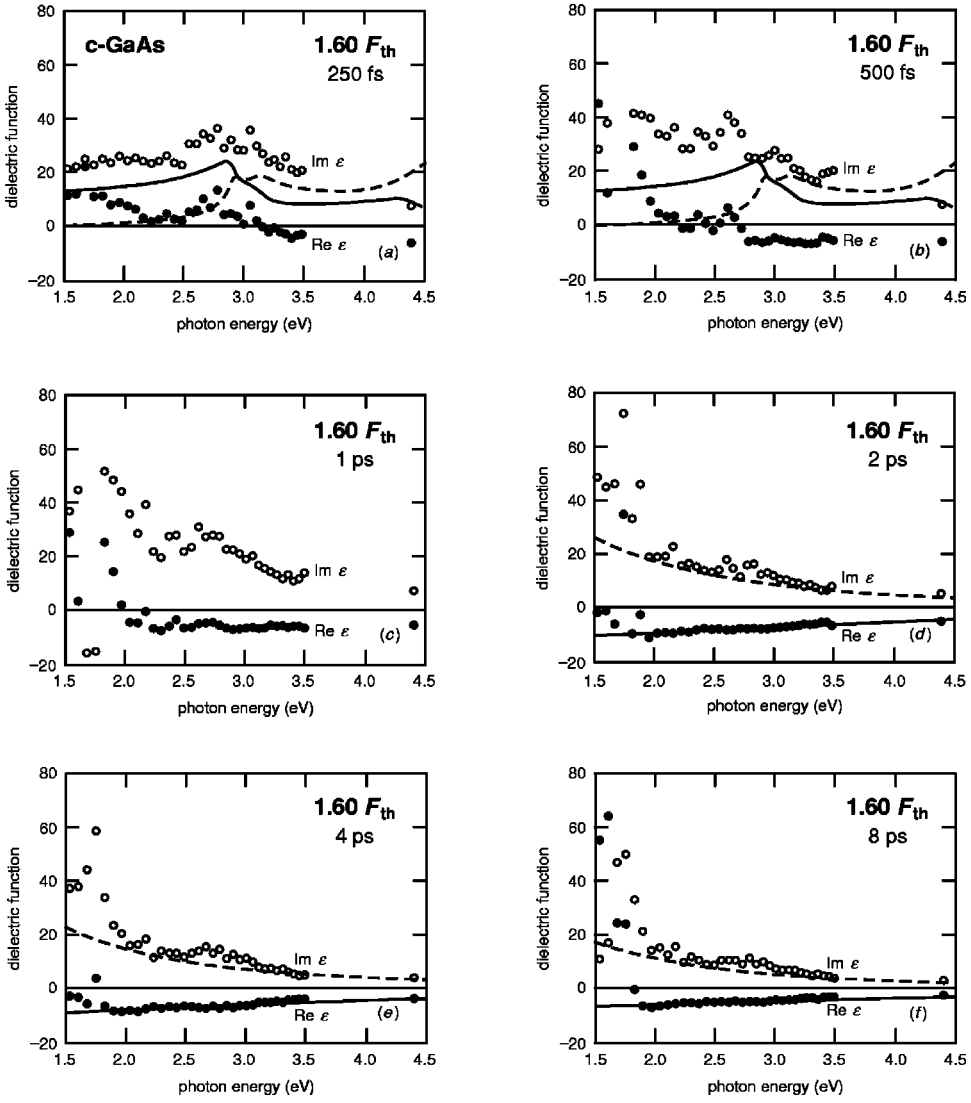


FIG. 6. Evolution of the dielectric function of *c*-GaAs (● $=\mathrm{Re}[\epsilon(\omega)]$, ○ $=\mathrm{Im}[\epsilon(\omega)]$) after excitation at $1.60F_{\text{th-}c}$. The curves in (a) and (b) show $\mathrm{Re}[\epsilon(\omega)]$ (solid line) and $\mathrm{Im}[\epsilon(\omega)]$ (dashed line) for *c*-GaAs at room temperature (Ref. 13). The curves in (d), (e), and (f) show Drude-model dielectric functions with 0.18-fs relaxation time and plasma frequencies of 13.0, 12.0, and 10.5 eV, respectively.

frequency indicates that the band gap is completely closed and that a semiconductor-to-metal transition has occurred.

We observe this semiconductor-to-metal transition at all fluences above $0.8F_{\text{th-}c}$. Figure 7 shows the drop in the zero crossing of $\mathrm{Re}[\epsilon(\omega)]$ versus time at different fluences, tracking the collapse of the bonding-antibonding gap. Once the zero-crossing photon energy goes below 2 eV, it is difficult to determine where the crossing occurs because the data are often noisy at the edges of the probe continuum.

Although the Drude fits are excellent, a peak centered at 2.75 eV is visible in Figs. 6(d)–6(f). This peak implies a contribution due to interband transitions, even after the band gap has collapsed. The same phenomenon occurs in copper, whose dielectric function is well described by a Drude model except for interband transitions above 2 eV that are responsible for the characteristic color of copper.

### *2. Amorphous gallium arsenide* ($F > 3.2F_{th\text{-}a}$)

Figure 8 shows the evolution of $\epsilon(\omega)$ for a pump fluence of $5.7F_{\text{th-}a}$; the response of the dielectric function is similar at other fluences above $3.2F_{\text{th-}a}$. At 500 fs the data already show a Drude-like metallic behavior, indicating the material

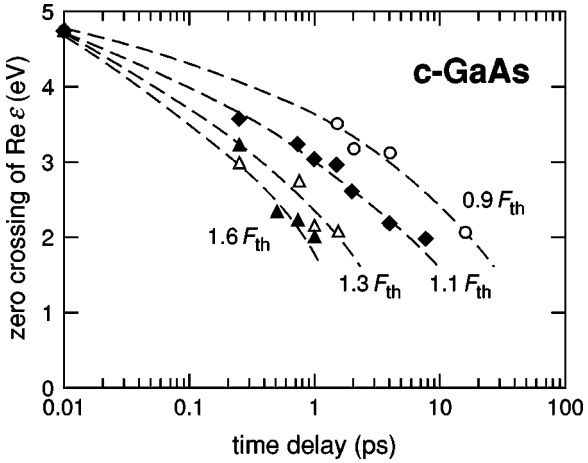


FIG. 7. Photon energy at which $\mathrm{Re}[\epsilon(\omega)]=0$ as a function of time delay for *c*-GaAs: $0.9F_{\text{th-}c}$ (○), $1.1F_{\text{th-}c}$ (◆), $1.3F_{\text{th-}c}$ (△), and $1.6F_{\text{th-}c}$ (▲). The dashed curves are guides to the eye.

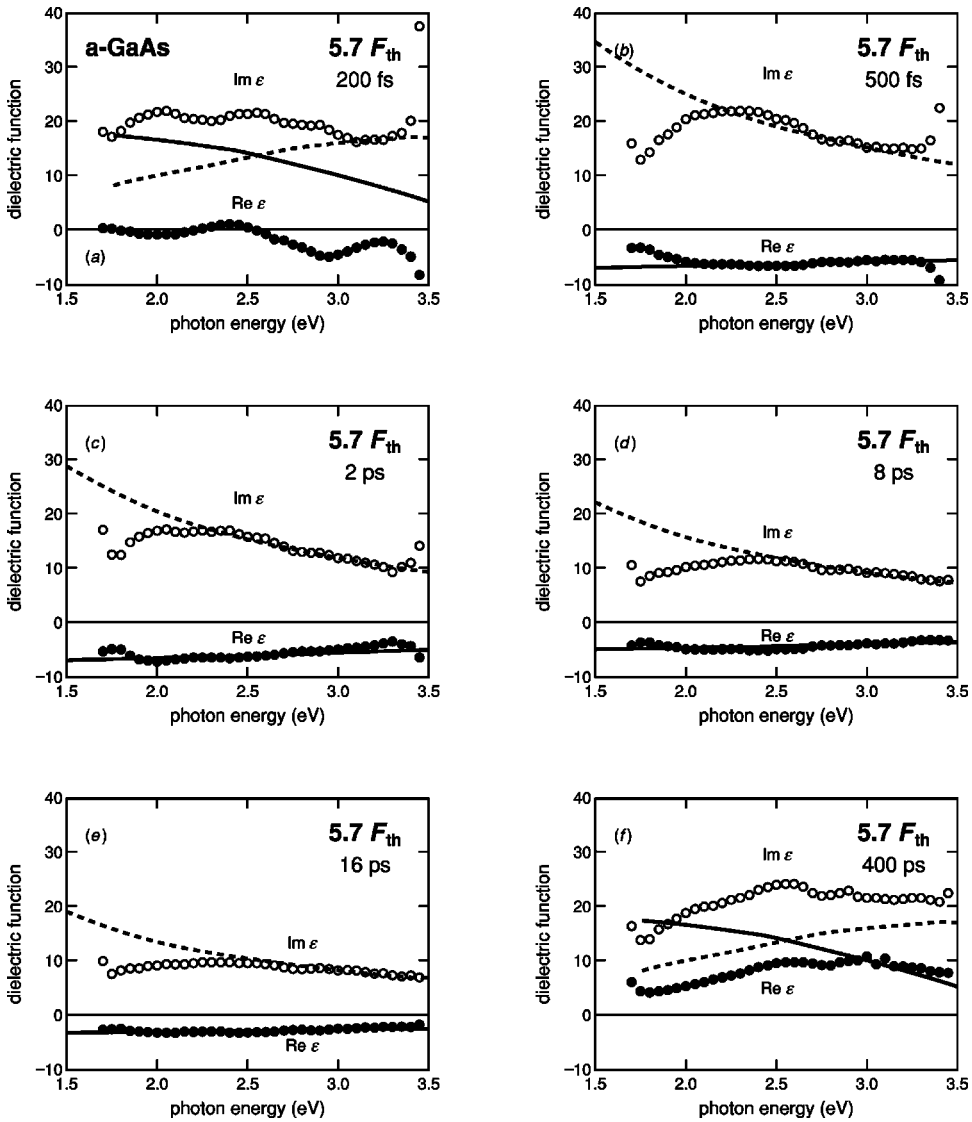


FIG. 8. Evolution of the dielectric function of *a*-GaAs (● = Re[$\epsilon(\omega)$], ○ = Im[$\epsilon(\omega)$]) after excitation at $5.7F_{\text{th-}a}$. The curves in (a) and (f) show Re[$\epsilon(\omega)$] (solid lines) and Im[$\epsilon(\omega)$] (dashed lines) for *a*-GaAs at room temperature (Ref. 15). The curves in (b), (c), (d), and (e) show Drude-model dielectric functions with plasma frequencies of 19.0, 16.0, 14.0, and 14.0 eV and relaxation times of 0.10, 0.12, 0.12, and 0.10 fs, respectively.

has undergone a nonthermal semiconductor-to-metal transition. The free parameters used in the Drude fit are the plasma frequency $\omega_p = 19.0$ eV and the relaxation time $\tau = 0.10$ fs. Between 1 ps and 16 ps, the relaxation time remains constant at 0.12 fs while the plasma frequency decreases—to 16.0 eV at 2 ps and 14.0 eV at 8 ps. At 16 ps, the best-fit value of $\tau$ decreases to 0.10 fs, while $\omega_p$ remains at 14.0 eV. By this time, the material is in thermal equilibrium and the dielectric function is that of the liquid phase. Between 50 ps and 400 ps, enough heat diffuses from the surface layer to cause resolidification, which is visible in the dielectric function at 400 ps.

Figure 8(b) shows that the transition to the metallic state is complete within 500 fs. To determine the duration of the semiconductor-to-metal transition, we plot five sets of dielectric function data at $5.7F_{\text{th-}a}$ around zero time delay without correcting for the probe chirp (see Fig. 9). The earliest probe data set ($-667$ fs) matches the dielectric function of *a*-GaAs because all probe wavelengths arrive before the pump pulse. In the latest data set (667 fs), the probe arrives more than 500 fs after the pump, so metallic behavior is observed at all wavelengths. The data set marked "0 fs" shows that the transition proceeds smoothly from the semiconducting state to the metallic one, beginning at $-50$ fs and ending at $+170$ fs on the chirp (upper horizontal) axis for a total duration of 220 fs. This duration is between that at $14F_{\text{th-}a}$ (170 fs) and $3.2F_{\text{th-}a}$ (380 fs).

## IV. DISCUSSION

### A. Carrier dynamics

Assuming linear absorption, a pump pulse at the threshold fluence of $F_{\text{th-}c} = 1.0$ kJ/m$^2$ excites about 10% of the valence electrons to the conduction band corresponding to a carrier density of about $10^{22}$ cm$^{-3}$. The excited free carriers affect both intraband and interband contributions to the dielectric function. First, free carriers affect the dielectric function via free-carrier absorption of the probe, as described by the Drude model. Second, screening of the ionic potential by free carriers and electronic many-body effects change the band structure,[25] which in turn affect the dielectric function. These free-carrier effects arise immediately after the excitation and dominate the changes in $\epsilon(\omega)$ for up to a picosec-

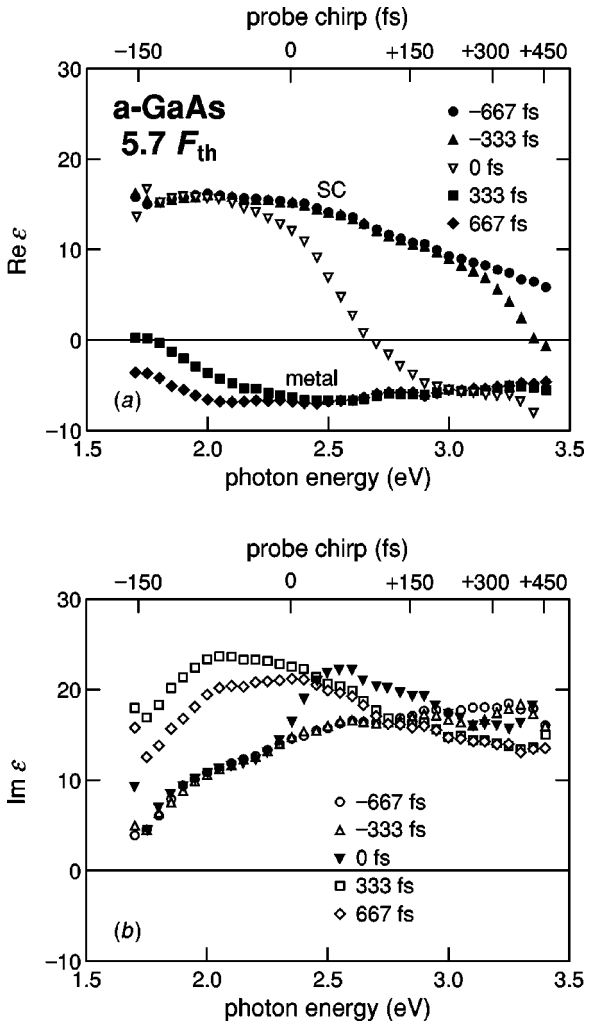


FIG. 9. Evolution of (a) Re$[\epsilon(\omega)]$ and (b) Im$[\epsilon(\omega)]$ when pulses of $5.7F_{\text{th-}a}$ excite *a*-GaAs, for positions of the time delay stage near time zero. The nonlinear probe chirp is indicated at the top of each plot. The legend gives the time delay at 2.35 eV.

ond after excitation, before changes in the lattice become important. Later, heating and disordering of the lattice alter the dielectric function through changes in the allowed energy states for free carriers.

Because the dielectric function is determined by the band structure, its evolution provides information on the carrier dynamics such as interactions between carriers at specific points in the Brillouin zone or scattering events from one point in the Brillouin zone to another. Due to the lack of crystal symmetry, a Brillouin zone cannot be defined for *a*-GaAs and so the following discussion of carrier dynamics is limited to *c*-GaAs.

#### *1. Low-fluence regime*

At short pump-probe delays the most pronounced feature in the dielectric function of *c*-GaAs is the decrease and broadening of the $E_1$ peak in Im$[\epsilon(\omega)]$ (see Fig. 1). The $E_1$ peak arises from 3-eV transitions in regions of $k$ space around the $L$ points and part way along the $L$-$\Gamma$ axes of the Brillouin zone (which we will refer to as the ''$L$ valleys'' due

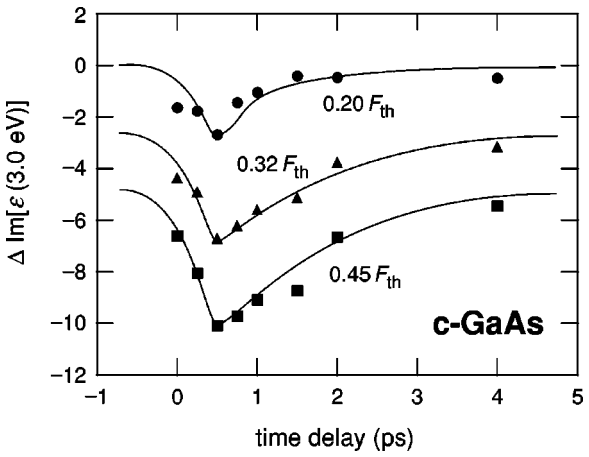


FIG. 10. Temporal evolution of the electronic contribution to Im$[\epsilon(\omega)]$ at 3.0 eV for $0.20F_{\text{th-}c}$ (●), $0.32F_{\text{th-}c}$ (▲), and $0.45F_{\text{th-}c}$ (■) obtained by taking the difference between the measured value and the curves in Fig. 1. The curves are guides to the eye, and each data series is shifted down by 2.5 with respect to the previous one.

to the curvature of the conduction band in these regions around the $L$ points), and the pump-induced decrease in absorption is caused by the presence of excited carriers in the $L$ valley by a number of different effects. First, Pauli blocking directly inhibits further absorption into the occupied states. Second, because excitons account for a substantial amount of absorption in semiconductors,[26,27] bleaching of the excitonic absorption also contributes to decreasing the overall absorption. Both screening and exchange interactions bleach excitonic absorption, and also the Coulomb enhancement of the excitonic absorption is reduced due to the excited carriers.[28,29] All of these effects are strongest at points close to the wave vector of the excited carriers because of the $|k_1-k_2|^{-1}$ dependence of the Coulomb potential. The reduction in absorption around the $E_1$ peak therefore indicates that carriers are present in the $L$ valley. Because the 1.9-eV photons in the pump beam excite the carriers into the $\Gamma$ valley, we can deduce the $\Gamma$-$L$ scattering from the evolution of the $E_1$ peak. The curves in Fig. 10 represent the purely electronic contribution to changes in Im$[\epsilon(\omega)]$ at the $E_1$ peak, as determined by subtracting the values for Im$[\epsilon(\omega)]$ predicted by exponential heating (see Figs. 1 and 2) from the measured values. As expected, the difference is largest at higher fluences when more free electrons are excited. The initial decrease in $\Delta$ Im$[\epsilon(3.0\text{ eV})]$ indicates a $\Gamma$-to-$L$ scattering time of a few hundred femtoseconds, confirming previous experimental findings,[30,31] but contradicting other findings of a few tens of femtoseconds.[32] Theoretical work by Zollner *et al.* partially reconciles the differences in the experimental results by introducing a temperature dependence of the $\Gamma$-$L$ scattering time.[33] However, according to the theory there is a lower bound of about 150 fs for the scattering time, further supporting our findings.

Free carriers relax through a combination of phonon emission, Auger recombination, radiative recombination, and carrier diffusion. The data in Figs. 1, 2, and 10 show that the effects of free carriers on $\epsilon(\omega)$ subside within 4 ps, whereas the lattice heats in 7 ps. This discrepancy in time scales

TABLE I. Comparison of deposited laser energy $E_{dep}$ with observed lattice heating $\Delta T_{latt}$ in the low-fluence regime. The lattice temperatures are the values measured at a pump-probe delay of 8 ps.

| $F$ | $E_{dep}$ (kJ/cm$^{-3}$) | $\Delta T_{latt}$ (K) | $\rho C_V \Delta T_{latt}$ (kJ/cm$^{-3}$) |
|---|---|---|---|
| $0.20F_{th}$ | 0.48 | 175 | 0.32 |
| $0.32F_{th}$ | 0.80 | 425 | 0.77 |
| $0.45F_{th}$ | 1.13 | $>475$ | $>0.87$ |

suggests that Auger recombination is the dominant relaxation mechanism in the first 10 ps. Auger recombination reduces the carrier density and hence the electronic effects on $\epsilon(\omega)$, without affecting the total carrier energy. Because the average energy per carrier increases, however, each remaining carrier must emit more phonons to reach the band edge, increasing the energy relaxation time and hence the lattice heating time. The lifetime of nonequilibrium LO phonons generated by carrier relaxation, which was found to be 4 ps in earlier work,[6] may also contribute to the delayed lattice heating time observed. However, its role at high carrier densities is not clear because phonon dynamics are complicated by higher-order processes such as plasmon-phonon coupling, phonon reabsorption, and phonon-phonon interactions.

Further evidence for delayed Auger heating can be obtained by comparing the energy density deposited by the laser in the excited volume with the energy density required for the observed lattice heating to occur throughout the excited region. These data are summarized in Table I for three excitations in the low-fluence range. The deposited energy density is

$$\mathcal{E}_{absorbed} = F(1-R)\ \alpha, \tag{1}$$

where $R=0.23$ is the (measured) reflectivity of the sample at 635 nm and $\alpha=[270\ \text{nm}]^{-1}$ the inverse of the absorption depth. The thermal energy density is

$$\mathcal{E}_{therm} = \rho\ \ C_V\ \ \Delta T, \tag{2}$$

where $\rho \approx 5.3$ g/cm$^3$ is the mass density of GaAs at room temperature, and $C_V \approx 250$ mJ/g K is the specific heat at constant volume.[24] There are two interesting points to note from Table I. First, the final lattice temperature increases nonlinearly with fluence. Therefore, a greater portion of the absorbed energy goes to lattice heating at higher fluences. Second, the fraction of absorbed energy going into lattice heating is surprisingly high, because electrons excited from the valence band are initially only 0.5 eV above the bottom of the conduction band, which corresponds to only about 25% of the laser photon energy.

This observed lattice heating behavior can be explained by Auger recombination. In an Auger event, an excited electron-hole pair recombines, transferring the entire 1.9 eV of excitation energy to an already excited electron (hole), pushing it higher in the conduction band (lower in the valence band). Auger recombination therefore makes it possible to transfer more than 25% of the absorbed laser energy to the lattice. Furthermore, the Auger rate increases with carrier density,[34] accounting for the increasing fraction of absorbed energy going to lattice heating at higher fluences.

The delayed Auger heating model of carrier relaxation is consistent with other experiments[35] and with theoretical predictions.[34] For the carrier densities in our experiments, Auger recombination dominates radiative recombination,[36] and carrier diffusion is limited by carrier confinement.[37] Assuming a simple picture of Auger recombination where the density changes as $dn/dt = -Cn^3$,[34] we determine the Auger coefficient to be $C = 10^{-31}$ cm$^6$/s. This is one order of magnitude lower than the result measured in previous low-density experiments.[36] However, screening is expected to limit the Auger rate at high carrier densities and our estimate of the Auger coefficient is consistent with the theoretical prediction of Yoffa.[34]

In summary, we find the following picture of carrier scattering and relaxation in the low-fluence regime of *c*-GaAs: (1) the excited carriers undergo intervalley scattering within a few hundred femtoseconds after excitation and (2) the dominant relaxation mechanism is Auger recombination, causing a delayed heating of the lattice and transferring a large fraction of absorbed energy to lattice heating.

#### *2. Medium- and high-fluence regimes*

As the fluence increases above $0.5F_{th\text{-}c}$ and the excited carrier density exceeds $5\times10^{21}$ cm$^{-3}$, the dielectric function changes due to a combination of many-body effects and a Drude contribution to $\epsilon(\omega)$. Kim *et al.* calculated the change in band structure in *c*-GaAs caused by a high density of free carriers through two many-body terms:[25] (1) screening of the ionic potential and (2) self-energy corrections arising from exchange-correlation effects. Both of these terms broaden interband transitions and reduce energy gaps, consistent with the broadening and slight downward shift of the $E_1$ peak that we observe in the first 500 fs after an excitation of $0.7F_{th\text{-}c}$ (see Fig. 4). The calculation of Kim and co-workers predicts large decreases in band gap with increasing carrier density. At an excited carrier density of about $2\times10^{22}$ cm$^{-3}$, or 10% of the valence electrons, the *L* valley minimum falls below the valence band maximum at $\Gamma$, closing the gap completely. The calculated decrease in the gaps at L and *X* is consistent with the observed decrease in bonding-antibonding gap from 4.75 eV to our spectral range of 1.7–3.4 eV above $0.8F_{th\text{-}c}$ (see Fig. 6). It is worth mentioning that many-body effects such as band gap renormalization have characteristic onset times on the order of the period of one plasma oscillation of the excited carrier distribution. For the excited carrier densities in our experiments these periods are less than 10 fs, which is below the temporal resolution of our apparatus. Thus the onset of such effects is instantaneous for all practical purposes in our experiments.

### B. Structural dynamics

#### *1. Low-fluence regime*

At low fluences the structural dynamics are simple: the lattice heats in a few picoseconds and then cools due to thermal diffusion. Conventional heating (in which a material re-

mains in thermodynamic equilibrium at all times) causes both expansion of the lattice and increased vibrational motion. Such a density change is necessary to maintain thermodynamic equilibrium. Models of the dielectric function of heated semiconductors suggest that during conventional heating, the change in $\epsilon(\omega)$ is mainly due to lattice vibrations, not density changes.[17,18] Does the observation that $\epsilon(\omega)$ of laser-irradiated *c*-GaAs at 4 ps matches that of heated *c*-GaAs imply that thermodynamic equilibrium occurs on this timescale? The information provided by time-resolved x-ray diffraction addresses the issue of lattice expansion.[38–40] Chin *et al.* observe a delay of about 10 ps in the onset of lattice expansion in InSb. Lattice expansion nucleates at the surface and a strain wave propagates into the material at the speed of sound—approximately 5 km/s in InSb.[39,40] Thus, it takes 20 ps for the lattice to expand down to a 100-nm depth (the approximate skin depth of our probe), and thermal equilibrium cannot be reached within 20 ps after excitation in our experiments. The ability to match the optical properties of laser-irradiated c-GaAs to those of conventionally heated c-GaAs for time delays as short as 4 ps points to an interesting picture of nonthermal heating. The generation of the acoustic phonons that cause lattice expansion occurs through decay of LO phonons and is delayed by the LO-phonon lifetime of several picoseconds.[6] Four picoseconds after excitation, most phonons in the material are new phonons that are emitted by hot electrons. It therefore follows that a distribution of nonequilibrium LO phonons has the same effect on the dielectric function of the material as an equilibrium distribution of phonons obtained by thermal heating would have. Future theoretical work could validate this picture by repeating the calculations of Gopalan *et al.*[18] while selectively considering the contributions of LO phonons and acoustic phonons to the changes in the dielectric function.

#### *2. Medium-fluence regime*

In the medium-fluence regime, the shape of $\epsilon(\omega)$ of excited *c*-GaAs in Fig. 4 is remarkably similar to $\epsilon(\omega)$ of *a*-GaAs, but the dielectric function is shifted to lower energies as one would expect for heated *a*-GaAs. There are no data for $\epsilon(\omega)$ of heated *a*-GaAs in the literature. From the low-fluence data for *c*-GaAs we infer that the $\epsilon(\omega)$ of *a*-GaAs at low excitation fluences is likely identical to the dielectric function of thermally heated *a*-GaAs. As expected for a hot material, these dielectric functions are shifted to lower photon energies relative to room-temperature *a*-GaAs, as shown in Fig. 3. Assuming that the density and specific heat of *a*-GaAs are those of *c*-GaAs (Ref. 24) (see Sec. IV A 1), Eqs. (1) and (2) predict that the temperature of *a*-GaAs should rise by 550 K after an excitation of $0.9F_{\text{th-}a}$, assuming that all of the absorbed energy is converted to thermal energy within the excited region. The low-fluence $\epsilon(\omega)$ data for *a*-GaAs can therefore serve as data for thermally heated *a*-GaAs.

The dielectric function of *c*-GaAs in the medium-fluence regime closely matches that of *a*-GaAs excited at low pump fluences. Figure 11, for example, shows the excellent agreement between $\epsilon(\omega)$ for *c*-GaAs at $F=0.7F_{\text{th-}c}$ and $\epsilon(\omega)$ measured for *a*-GaAs at $F=0.9F_{\text{th-}a}$ at a time delay of 4 ps. This agreement confirms that, for medium fluences, *c*-GaAs undergoes a transition to a heated disordered solid phase similar to the heated amorphous phase.

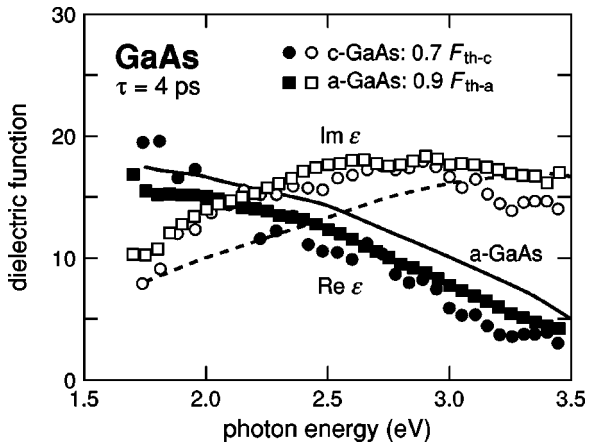


FIG. 11. Comparison of the dielectric function of *c*-GaAs in the medium-fluence regime with that of *a*-GaAs in the low-fluence regime, 4 ps after excitation. The curves show $\epsilon(\omega)$ (solid line $=\text{Re}[\epsilon(\omega)]$, dashed line$=\text{Im}[\epsilon(\omega)]$) for *a*-GaAs at room temperature (Ref. 15).

Nonthermal disordering or ''nonthermal melting'' by strong electronic excitation was first suggested in 1979 by van Vechten *et al.*[41,42] Since then, nonthermal melting upon irradiation with ultrashort laser pulses has been observed in a number of experiments in a variety of materials, mainly by observing the reflected second-harmonic signal from the material.[20,43–47]

The experimental results were supported by theoretical work on lattice instabilities caused by strong electronic excitation.[48–50] More recent findings report the observation of the onset of nonthermal melting by tracking the softening of phonon modes due to a induced lattice instability.[51] Our results not only demonstrate a complementary technique that allows one to observe the nonthermal disordering process, but also provide insight into the final state of the material.

We can estimate the crystallization energy of GaAs from the excitation conditions at which $\epsilon(\omega)$ of *c*-GaAs and *a*-GaAs agree (cf. Fig. 11). The crystallization energy—the energy required to order *a*-GaAs into *c*-GaAs—is equal to the difference between the energy required to disorder *c*-GaAs and the energy required to heat *a*-GaAs to the same heated disordered state. At 4 ps time delay, the dielectric function of *c*-GaAs at $0.7F_{\text{th-}c}$ and that of *a*-GaAs at $0.9F_{\text{th-}a}$ are identical. Using the fact that a pump fluence of 1 kJ/m$^2$ corresponds to a deposited energy of about 16.4 kJ/mol (counting both gallium and arsenic ions as individual atoms), we determine the crystallization energy to be $10 \pm 3$ kJ/mol. The error arises from uncertainty in the measurement of absolute values of the pump fluence. Our result is consistent with experimental and theoretical estimates for other tetrahedrally coordinated semiconductors. Donovan *et al.* reported values of 11.6 kJ/mol for Ge and 13.4 kJ/mol for Si.[52]

### *3. High-fluence regime*

In the high-fluence regime, our data provide direct evidence for nonthermal structural change. For both *c*-GaAs and *a*-GaAs we observe a transition to a metallic phase within a few picoseconds. For both materials, the nonthermal transition occurs more rapidly as the fluence increases. For *a*-GaAs at $14F_{\text{th-}a}$, the transition to the metallic state takes only 170 fs. Likewise, the crystalline phase undergoes a phase transition in about 260 fs when the excitation fluence is about 17 times the threshold for permanent change in *c*-GaAs. Although model calculations predict that the gap in *c*-GaAs disappears completely when 10% of the valence electrons are excited,[25] they cannot account for the time dependence of our data. If the band gap change were caused only by free-carrier effects, the gap would be smallest immediately after excitation, when the carrier density is largest, and would subsequently grow, as the carriers relax. However, for fluences above $0.8F_{\text{th-}c}$, we observe a gradual drop in the zero crossing of $\text{Re}[\epsilon(\omega)]$ over several picoseconds. On the other hand, band structure modifications caused by many-body effects depend on carrier temperature as well as density, and the carrier temperature changes with time. Theoretical work by Zimmermann and others[53,54] indicates that band-gap renormalization is only weakly dependent on carrier temperature at carrier densities of $10^{23}$ cm$^{-3}$. Thus we conclude that electronic effects cannot be solely responsible for the observed decrease in the gap over several picoseconds; structural changes must be the dominant cause.

This is not to say that direct electronic effects do not occur: effects such as screening of the ions and the self-energy correction due to carrier-carrier interactions are present.[25] However, these direct electronic effects cannot account for all the changes we observe. One might expect that above some fluence the numbers of carriers excited is sufficient to cause the band gap in GaAs to close due to electronic effects alone. Thus, it will be interesting to conduct experiments at even higher fluences than those reported here, to search for a transition to the metallic state within the femtosecond pump pulse duration. Such a rapid transition would be driven solely by electronic effects because the lattice structure cannot change on this timescale.

The observed structural changes are nonthermal because the semiconductor-to-metal transition occurs in less than 2 ps, that is, before electrons have fully equilibrated with the lattice. The following mechanism has been proposed for femtosecond-laser-induced nonthermal structural changes in semiconductors.[41,48–50,55–57] The laser excitation promotes electrons from bonding states in the valence bands to antibonding states in the conduction bands. This weakens the lattice bonding and the atoms move to new equilibrium positions. If the excitation is sufficiently strong, lattice instability leads to deformation of the zinc blende structure and to a metallic transition.[50,56] Stampfli and Bennemann estimate that an excitation of about 10% of the carriers is sufficient to cause a semiconductor-to-metal transition in GaAs or Si, in agreement with our data. In recent work, Graves, Dumitrica, and Allen use molecular dynamics simulations to predict how the dielectric function of *c*-GaAs changes during the transition following the excitation by a fs laser pulse.[56,57] Their results are in qualitative agreement with our data. Within a few hundred femtoseconds, the simulations indicate lattice disordering and the calculated dielectric function matches the Drude model quite well. Furthermore, both experiment and simulation show a residual interband contribution around 2.5–3.0 eV after the semiconductor-to-metal transition has occurred. The simulations suggest that this contribution arises from some of the states in the valence and conduction bands which originally produced the $E_2$ peak in unexcited *c*-GaAs, but which are much closer together as a result of the excitation and consequent band-gap collapse.

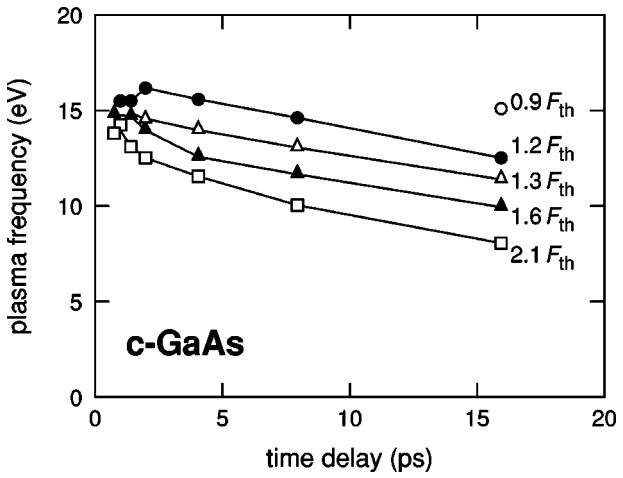


FIG. 12. Plasma frequency as a function of time delay in the high-fluence regime for *c*-GaAs: $0.9F_{\text{th-}c}$ (○), $1.2F_{\text{th-}c}$ (●), $1.3F_{\text{th-}c}$ (△), $1.6F_{\text{th-}c}$ (▲), and $2.1F_{\text{th-}c}$ (□). The Drude-model fits that produce these values of $\omega_p$ all yield a relaxation time $\tau = 0.15$ fs. The lines joining the data on the plot are guides to the eye.

Figures 12 and 13 show the evolution of the metallic state for *c*-GaAs and *a*-GaAs in the high-fluence regime by track-

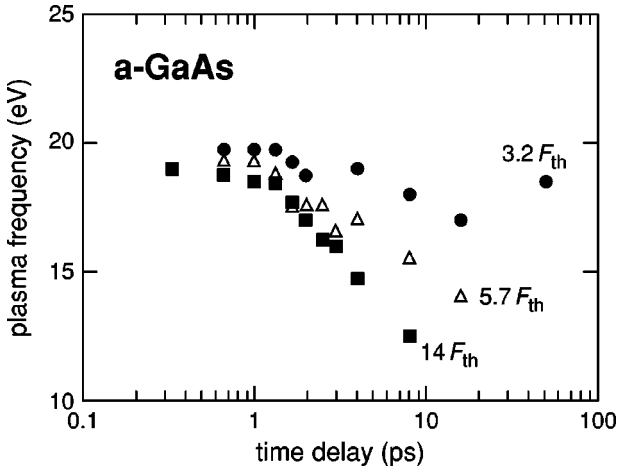


FIG. 13. Plasma frequency $\omega_p$ as a function of time delay for different excitations in the high-fluence regime for *a*-GaAs: $3.2F_{\text{th-}a}$ (●), $5.7F_{\text{th-}a}$ (△), and $14F_{\text{th-}a}$ (■). The Drude-model fits to the dielectric function data that produce the values of $\omega_p$ all yield a relaxation time $\tau = 0.10$ fs.

ing the plasma frequency versus time. Two striking phenomena become apparent: first, the plasma frequency decreases over time, and second, the plasma frequency is lower for higher fluences. These patterns of behavior appear to be universal. We observe nonthermal transitions to a metallic state, followed by a decrease in plasma frequency with time, and lower plasma frequencies at higher fluences, for other semiconducting materials as well.[58]

The decrease in plasma frequency with time is most likely due to diffusion of carriers into the material. Because the probe beam only probes the first 10 nm in the metallic state, carriers diffuse very rapidly out of the probed region. Taking literature values for the diffusion coefficient in *c*-GaAs,[59] the carrier density of the probed region is reduced by half in 4 ps. An electron plasma expanding out of the material could also cause a decrease in plasma frequency. However, the residual interband transitions in the dielectric function data indicate that most of the probe reaches the sample and is not obscured by a plasma in front of the sample. Thus we conclude that carrier diffusion into the sample causes the observed decline in plasma frequency over time.

The decrease in plasma frequency with increasing fluence is surprising because, once the band gap collapses, all valence electrons should be free, independent of fluence. Note, however, that the plasma frequency depends not only on the carrier density $N$ but also on the effective masses $m$ of the free carriers:[22]

$$\omega_p = \left[ \frac{Ne^2}{\epsilon_0 \, m} \right]^{1/2}. \tag{3}$$

Our data thus suggest that the effective masses of carriers increase with fluence, causing a decrease of the plasma frequency. Future simulations might be able to calculate effective masses and plasma frequencies at different fluences, in order to elucidate the dynamics in Figs. 12 and 13.[60]

## V. CONCLUSIONS

The time-resolved dielectric function provides a wealth of new information on the electron dynamics and the nature of structural changes in GaAs following femtosecond laser excitation of 1%–10% of the valence electrons. For *c*-GaAs we distinguish three regimes of behavior depending on the excitation fluence. Below 0.5 kJ/m$^2$, the excited free carriers scatter from the $\Gamma$ valley to side valleys within a few hundred femtoseconds. They relax by rapid Auger recombination and subsequent phonon emission. Above 0.5 kJ/m$^2$, the initial electronic effects on $\epsilon(\omega)$ are larger but more difficult to interpret. The excited carriers affect the dielectric function through a combination of free carrier absorption, band filling, and changes in the band structure due to ionic screening and other many-body effects. After a few picoseconds, the lattice disorders. These structural changes may be thermal or nonthermal below the semiconductor-to-metal transition threshold, 0.8 kJ/m$^2$, but above this threshold the changes must be nonthermal because they start before carrier relaxation is complete.

Our data show similarities in the response of *a*-GaAs and *c*-GaAs to intense femtosecond excitation. At low fluences, we see evidence of heating in *a*-GaAs, as we observe for *c*-GaAs. For fluences above about 0.32 kJ/m$^2$ (or $3F_{\text{th-}a}$), *a*-GaAs undergoes a transition to a metallic phase similar to that reached by *c*-GaAs. At $14F_{\text{th-}a}$, the transition to the metallic state in *a*-GaAs takes just 170 fs, but is still long enough to indicate that the transition is structurally driven. Even at the highest available fluences, we do not observe a purely electronically driven band-gap collapse—a collapse within the duration of the pump pulse—in either the crystalline or the amorphous material.

For both materials we observe a decrease in plasma frequency over time after the metallic phase appears, as well as lower plasma frequencies at higher pump fluences. Comparing the dielectric function data for the crystalline and amorphous material we can estimate the crystallization energy of GaAs to be about 10 kJ/mol.

Finally it is worth noting that the boundary between the low- and high-fluence regimes is nearly the same for *c*-GaAs and *a*-GaAs (0.5 and 0.3 kJ/m$^2$, respectively), indicating that the fluence needed to drive the semiconductor-to-metal transition is independent of the original structure of the material. The threshold fluence for permanent damage, however, differs by an order of magnitude—1 kJ/m$^2$ for *c*-GaAs and 0.1 kJ/m$^2$ for *a*-GaAs. This observation implies that an order of magnitude less energy is required to drive the crystalline-to-amorphous transition than the amorphous-to-amorphous transition in GaAs.

## ACKNOWLEDGMENTS

We gratefully acknowledge Dr. C. W. White of Oak Ridge National Laboratory for providing the *a*-GaAs sample. We thank Professor R. E. Allen, Professor M. J. Aziz, Dr. L X. Benedict, and Professor H. Ehrenreich for fruitful discussions.

[1] D.S. Chemla, Phys. Today **46** (6), 46 (1993).
[2] I.S. Ruddock and D.J. Bradley, Appl. Phys. Lett. **29**, 296 (1976).
[3] J. Shah, *Ultrafast Spectroscopy of Semiconductors and Semiconductor Nanostructures* (Springer-Verlag, Berlin, 1996).
[4] C. Lawetz, J.C. Cartledge, C. Rolland, and J. Yu, J. Lightwave Technol. **15**, 697 (1997).
[5] J.E. Cunningham, Mater. Sci. Eng., R. **25**, 155 (1999).
[6] J.A. Kash, J.C. Tsang, and J.M. Hvam, Phys. Rev. Lett. **54**, 2151 (1985).
[7] W.W. Chow and R.R. Craig, IEEE J. Quantum Electron. **27**, 2267 (1991).
[8] X. Liu, D. Du, and G. Mourou, IEEE J. Quantum Electron. **33**, 1706 (1997).
[9] J.P. Callan, A.M.-T. Kim, L. Huang, and E. Mazur, Chem. Phys. **251**, 167 (1998).
[10] A. M.-T. Kim, Ph.D. thesis, Harvard University, 2001.
[11] D. Beaglehole, Proc. Phys. Soc. London **85**, 1007 (1965).
[12] E.N. Glezer, Y. Siegal, L. Huang, and E. Mazur, Phys. Rev. B **51**,

6959 (1995).
[13] E.D. Palik, *Handbook of Optical Constants of Solids* (Academic Press, New York, 1985).
[14] H. Yao, P.G. Snyder, and J.A. Woollam, J. Appl. Phys. **70**, 3261 (1991).
[15] M. Erman, J.B. Theeten, P. Chambon, S.M. Kelso, and D.E. Aspnes, J. Appl. Phys. **56**, 2664 (1984).
[16] G.E. Jellison and F.A. Modine, Phys. Rev. B **27**, 7466 (1983).
[17] G.A. Samara, Phys. Rev. B **27**, 3494 (1983).
[18] S. Gopalan, P. Lautenschlager, and M. Cardona, Phys. Rev. B **35**, 5577 (1987).
[19] P. Baeri and S.U. Campisano, in *Laser Annealing of Semiconductors*, edited by J.M. Poate and J.W. Mayer (Academic Press, London, 1982).
[20] H.W.K. Tom, G.D. Aumiller, and C.H. Brito-Cruz, Phys. Rev. Lett. **60**, 1438 (1988).
[21] E.N. Glezer, Y. Siegal, L. Huang, and E. Mazur, Phys. Rev. B **51**, 9589 (1995).
[22] N.W. Ashcroft and N.D. Mermin, *Solid State Physics* (Saunders College, Philadelphia, 1976).
[23] W. A. Harrison, *Electronic Structure and the Properties of Solids*: *The Physics of the Chemical Bond* (Dover, New York, 1989).
[24] S. Adachi, *GaAs and Related Materials* (World Scientific, Singapore, 1994).
[25] D.H. Kim, H. Ehrenreich, and E. Runge, Solid State Commun. **89**, 119 (1994).
[26] S. Zollner, K.D. Myers, J.M. Dolan, D.W. Bailey, and C.J. Stanton, Thin Solid Films **313**, 578 (1998).
[27] P.Y. Yu and M. Cardona, *Fundamentals of Semiconductors* (Springer-Verlag, Berlin, 1996).
[28] S. Schmitt-Rink, C. Ell, and H. Haug, Phys. Rev. B **33**, 1183 (1986).
[29] H. Haug and S.W. Koch, Phys. Rev. A **39**, 1887 (1989).
[30] R.G. Ulbrich, J.A. Kash, and J.C. Tsang, Phys. Rev. Lett. **62**, 949 (1989).
[31] P.N. Saeta, J.F. Federici, B.I. Greene, and D.R. Dykaar, Appl. Phys. Lett. **60**, 1477 (1992).
[32] P.C. Becker, H.L. Fragnito, C.H. Brito-Cruz, J. Shah, R.L. Fork, J.E. Cunningham, J.E. Henry, and C.V. Shank, Appl. Phys. Lett. **53**, 2089 (1988).
[33] S. Zollner, S. Gopalan, and M. Cardona, Semicond. Sci. Technol. **7**, B137 (1992).
[34] E.J. Yoffa, Phys. Rev. B **21**, 2415 (1980).
[35] M.C. Downer and C.V. Shank, Phys. Rev. Lett. **56**, 761 (1986).
[36] U. Strauss, W.W. Rühle, and K. Köhler, Appl. Phys. Lett. **62**, 55 (1993).
[37] H.M. van Driel, Phys. Rev. B **35**, 8166 (1987).
[38] J. Larsson, P.A. Heimann, A.M. Lindenberg, P.J. Schuck, P.H. Bucksbaum, R.W. Lee, H.A. Padmore, J.S. Wark, and R.W. Falcone, Appl. Phys. A: Mater. Sci. Process. **66**, 587 (1998).
[39] C. Rose-Petruck, R. Jimenez, T. Guo, A. Cavalleri, C.W. Siders, F. Raksi, J.A. Squier, E.C. Walker, K.R. Wilson, and C.P.J. Barty, Nature (London) **398**, 310 (1999).
[40] A.H. Chin, R.W Schoenlein, T.E. Glover, P. Balling, W.P. Leemans, and C.V. Shank, Phys. Rev. Lett. **83**, 336 (1999).
[41] J.A. Van Vechten, R. Tsu, and F.W. Saris, Phys. Lett. **A74**, 422 (1979).
[42] J. A. Van Vechten, in *Laser and Electron Beam Processing of Semiconductors*, edited by C.W. White and P.S. Peercy (Academic Press, New York, 1980).
[43] C.V. Shank, R. Yen, and C. Hirlimann, Phys. Rev. Lett. **51**, 900 (1983).
[44] P. Saeta, J.-K. Wang, Y. Siegal, N. Bloembergen, and E. Mazur, Phys. Rev. Lett. **67**, 1023 (1991).
[45] S.V. Govorkov, I.L. Shumay, W. Rudolph, and T. Schröder, Opt. Lett. **16**, 1013 (1991).
[46] K. Sokolwski-Tinten, H. Schulz, J. Bialkowski, and D. von der Linde, Appl. Phys. A: Solids Surf. **53**, 227 (1991).
[47] K. Sokolwski-Tinten, H. Schulz, J. Bialkowski, and D. von der Linde, Phys. Rev. B **51**, 14 186 (1995).
[48] P. Stampfli and K.H. Bennemann, Phys. Rev. B **42**, 7163 (1990).
[49] P. Stampfli and K.H. Bennemann, Phys. Rev. B **46**, 10 686 (1992).
[50] P. Stampfli and K.H. Bennemann, Phys. Rev. B **49**, 7299 (1994).
[51] S. Hunsche, K. Wienecke, T. Dekorsy, and H. Kurz, Phys. Rev. Lett. **75**, 1815 (1995).
[52] E.P. Donovan, F. Spaepen, J.M. Poate, and D.C. Jacobson, Appl. Phys. Lett. **55**, 1516 (1989).
[53] R. Zimmermann, *Many Particle Theory of Highly Excited Semiconductors* (Teubner, Leipzig, 1988).
[54] H. Kalt and M. Rinker, Phys. Rev. B **45**, 1139 (1992).
[55] P. Silvestrelli, A. Alavi, M. Parrinello, and D. Frenkel, Phys. Rev. Lett. **77**, 3149 (1996).
[56] J.S. Graves and R.E. Allen, Phys. Rev. B **58**, 13 627 (1998).
[57] R.E. Allen, T. Dumitrica, and B. Torralva, in *Ultrafast Processes in Semiconductors*, edited by K.-T. Tsen (Academic Press, New York, 2000).
[58] J.P. Callan, A.M.-T. Kim, C.A.D. Roeser, and E. Mazur, Phys. Rev. B **64**, 073201 (2001).
[59] K. Seeger, *Semiconductor Physics*: *An Introduction* (Springer-Verlag, Berlin, 1991).
[60] The microscopic definition of effective mass (related to the curvature of the respective conduction band) only holds for the crystalline material. In case of amorphous GaAs, effective mass can only be viewed as a macroscopic parameter in the Drude model. Future theoretical work might shed more light on the microscopic nature of effective masses for metallic amorphous materials.